Quadrupole Order in the Frustrated Pyrochlore $Tb_{2+x}Ti_{2-x}O_{7+y}$

H. Takatsu,[1,2] S. Onoda,[3,4] S. Kittaka,[5] A. Kasahara,[5] Y. Kono,[5] T. Sakakibara,[5] Y. Kato,[3,6] B. Fåk,[7]
J. Ollivier,[7] J. W. Lynn,[8] T. Taniguchi,[1] M. Wakita,[1] and H. Kadowaki[1]

[1]*Department of Physics, Tokyo Metropolitan University, Hachioji-shi, Tokyo 192-0397, Japan*
[2]*Department of Energy and Hydrocarbon Chemistry, Graduate School of Engineering, Kyoto University, Kyoto 615-8510, Japan*
[3]*RIKEN Center for Emergent Matter Science (CEMS), Wako, Saitama 351-0198, Japan*
[4]*Condensed Matter Theory Laboratory, RIKEN, Wako, Saitama 351-0198, Japan*
[5]*Institute for Solid State Physics, University of Tokyo, Kashiwa 277-8581, Japan*
[6]*Department of Applied Physics, University of Tokyo, Bunkyo, Tokyo 113-8656, Japan*
[7]*Institute Laue Langevin, BP 156, F-38042 Grenoble, France*
[8]*NCNR, National Institute of Standards and Technology, Gaithersburg, Maryland 20899-6102, USA*
(Received 15 June 2015; revised manuscript received 4 April 2016; published 26 May 2016)

A hidden order that emerges in the frustrated pyrochlore $Tb_{2+x}Ti_{2-x}O_{7+y}$ with $T_c = 0.53$ K is studied using specific heat, magnetization, and neutron scattering experiments on a high-quality single crystal. Semiquantitative analyses based on a pseudospin-1/2 Hamiltonian for ionic non-Kramers magnetic doublets demonstrate that it is an ordered state of electric quadrupole moments. The elusive spin liquid state of the nominal $Tb_2Ti_2O_7$ is most likely a U(1) quantum spin-liquid state.

Geometrically frustrated magnets have been actively investigated in condensed matter physics [1]. In particular, spin ice (SI), e.g., $R_2Ti_2O_7$ (R = Dy or Ho) [2,3], provides prototypical frustrated Ising magnets with the pyrochlore lattice structure [4], consisting of a three-dimensional network of corner-sharing tetrahedra [Fig. 1(b)]. It displays fascinating features such as a finite zero-point entropy [5] and thermally excited emergent magnetic or SI monopoles [6,7]. An intriguing theoretical proposal for a U(1) quantum spin liquid (QSL) state [8] has been made for variants of SI endowed with quantum spin fluctuations [9–14]. The U(1) QSL state [8–10] is characterized by an emergent U(1) gauge field producing gapless fictitious photons and by gapped bosonic spinon excitations carrying the SI magnetic monopole charge [8,9,13,15]. By increasing the transverse interaction, the system can undergo a phase transition from the U(1) QSL to a long range ordered (LRO) state of transverse spins or pseudospins representing electric-quadrupole moments for non-Kramers ions [9–11]. This state can be described as a Higgs phase [16–20].

In a quest to QSL states in frustrated magnetic systems from both theoretical [21–23] and experimental [24,25] viewpoints, an Ising-like pyrochlore $Tb_2Ti_2O_7$ (TTO) is a potential candidate for a U(1) QSL: it has been reported to remain in a fluctuating spin state down to 50 mK without magnetic LRO [26,27]. However, the origin of this spin liquid state of TTO has been elusive for more than a decade despite many investigations (see Refs. [4,13,28] and references therein, and recent Refs. [29–31]), and is still under hot debate [13,28]. To solve this challenging problem of TTO, we start this investigation by postulating that the theoretically proposed interaction between electric quadrupole moments of non-Kramers ions including Tb^{3+} [the

fourth term of Eq. (1)] [11] is at work for giving the quantum fluctuations to TTO. This postulation is a natural consequence of the previous unsuccessful trial and error of explaining TTO by taking into account only the interactions between magnetic dipole moments [the first three terms of Eq. (1)] and the perturbation through first excited crystal-field (CF) states [14,32], and by taking another assumption of Jahn-Teller (JT) distortion [28,33]. Under the present postulation, two ground states of off-stoichiometric $Tb_{2+x}Ti_{2-x}O_{7+y}$ samples [34] will possibly
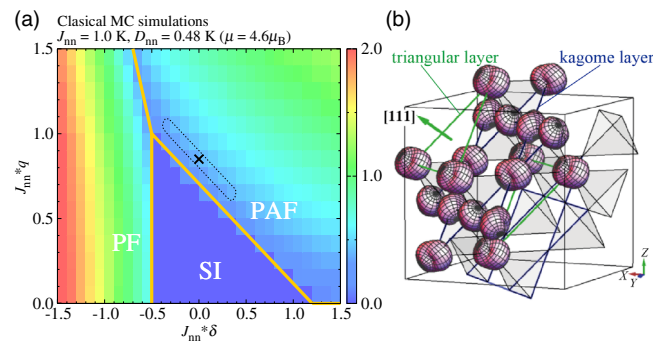

FIG. 1. (a) Phase diagram of the effective Hamiltonian Eq. (1) determined from CMC simulations. The shading (color) represents T_c. Two quadrupole LRO phases, the planar antiferropseudospin (PAF) and planar ferropseudospin (PF) phases, exist in the vicinity of the SI phase [11]. Classical SI is replaced by a U(1) QSL in quantum theory [9]. The region enclosed by the dotted line represents an acceptable parameter region for the experimental data on $Tb_{2.005}Ti_{1.995}O_{7+y}$. The cross mark indicates the typical values $(\delta, q) = (0, 0.85)$. (b) Schematic view of the deformation of the f-electron charge density due to the PAF order on the pyrochlore lattice.

be accounted for by the U(1) QSL ($x < x_c$) and electric quadrupolar ($x > x_c$) states of Ref. [9].

In this Letter, we investigate the hidden order of Tb$_{2+x}$Ti$_{2-x}$O$_{7+y}$ ($x = 0.005 > x_c$), because the electric quadrupolar order is more tractable than the U(1) QSL by using semiclassical theoretical analyses. Specific heat, magnetization, and neutron scattering experiments were performed, and these experimental data were analyzed using quantum and classical Monte Carlo (QMC, CMC) simulations, and a mean-field random-phase approximation (MF RPA). The results demonstrate that the hidden order is an electric quadrupolar order [Fig. 1(b)] and that the parameters of the model Hamiltonian are located close to a phase boundary between the electric quadrupole and U(1) QSL states [Fig. 1(a)], which suggests that the elusive spin-liquid state of TTO is the U(1) QSL. We emphasize that a high-quality single-crystalline sample with a well-controlled x value [35] enables us to accomplish this work.

An effective pseudospin-1/2 Hamiltonian [11] relevant for the non-Kramers magnetic doublets of TTO is

$$\mathcal{H} = J_{nn} \sum_{\langle r,r' \rangle} \sigma_r^z \sigma_{r'}^z - \mu_{eff} \boldsymbol{H} \cdot \sum_r \boldsymbol{e}_r^z \sigma_r^z$$

$$+ D r_{nn}^3 \sum \left[\frac{\boldsymbol{e}_r^z \cdot \boldsymbol{e}_{r'}^z}{|\boldsymbol{r} - \boldsymbol{r'}|^3} - \frac{3[\boldsymbol{e}_r^z \cdot (\boldsymbol{r} - \boldsymbol{r'})][\boldsymbol{e}_{r'}^z \cdot (\boldsymbol{r} - \boldsymbol{r'})]}{|\boldsymbol{r} - \boldsymbol{r'}|^5} \right] \sigma_r^z \sigma_{r'}^z$$

$$+ J_{nn} \sum_{\langle r,r' \rangle} [2\delta(\sigma_r^+ \sigma_{r'}^- + \sigma_r^- \sigma_{r'}^+) + 2q(e^{i2\phi_{r,r'}} \sigma_r^+ \sigma_{r'}^+ + \text{H.c.})].$$

(1)

Here, we consider only the CF ground-state doublet [30,36], and neglect the first excited doublet at $E \simeq 18$ K, since we are mainly interested in the low-T properties below 2 K. In Eq. (1), $\boldsymbol{\sigma}_r$ are the Pauli matrices (pseudospin) at a site $\boldsymbol{r}$, $\sigma_r^\pm \equiv (\sigma_r^x \pm i\sigma_r^y)/2$, and $\phi_{r,r'} = \pm(2\pi/3), 0$ [11,37]. The magnetic dipole moment $\mu_{eff}\sigma_r^z$ is parallel to the local $\langle 111 \rangle$ axis $\boldsymbol{e}_r^z$ [37]. The first three terms of Eq. (1) represent the nearest-neighbor (NN) exchange interaction, the Zeeman energy under a magnetic field $\boldsymbol{H}$, and the dipolar interaction, respectively. They constitute the classical dipolar SI Hamiltonian $\mathcal{H}_m$ [38]. It can be approximated [38,39] by the NN classical SI model $\mathcal{H}_{m,eff} = J_{nn,eff} \sum_{\langle r,r' \rangle} \sigma_r^z \sigma_{r'}^z - \mu_{eff} \boldsymbol{H} \cdot \sum_r \boldsymbol{e}_r^z \sigma_r^z$, where $J_{nn,eff} = J_{nn} + D_{nn}$ ($D_{nn} = \frac{5}{3}D$). The last term of Eq. (1) represents the quadrupole interaction $\mathcal{H}_q$. We note that the transverse components (σ_r^x, σ_r^y) of the pseudospin represent electric quadrupole (and 16-, 64-pole) moments [11,37]. Note that QMC simulations of the model Eq. (1) suffer from a negative sign problem. On the other hand, thermodynamic properties away from the QSL state, including phase transitions to the LRO phases, can be captured by CMC simulations semiquantitatively. Therefore, in most of the cases, we employ CMC simulations.

CMC simulations were performed up to 1024 pseudospins, in which the pseudospin $\boldsymbol{\sigma}_r$ is treated as a classical

unit vector [40]. The resulting zero-field phase diagram is shown in Fig. 1(a) for the case of $D_{nn} = 0.48$ K, namely, $\mu = 4.6 \, \mu_B$ [41], and $J_{nn} = 1.0$ K (this value of D_{nn} will be used throughout the Letter and the choice of J_{nn} will be explained further below). A quantum mechanical treatment using gauge mean-field (MF) theory shows that the classical SI phase region in Fig. 1(a) is mostly replaced by a U(1) QSL phase except at $\delta = q = 0$ [9]. The phase diagram has two quadrupole LRO phases originating from different ordering patterns of (σ_r^x, σ_r^y): planar antiferropseudospin (PAF) and planar ferropseudospin (PF) states denoted in the classical MF phase diagram (Fig. 7 in Ref. [11]). In particular, a deformation of the f-electron charge density [45] for the PAF phase is illustrated in Fig. 1(b) [9,40]. In the following, we will show that most of the experimental data on the high-quality polycrystalline and single-crystalline samples of TTO with $x = 0.005$ can be explained by choosing $J_{nn} = 1$ K, $\delta = 0$, and $q = 0.85$ within semiquantitative analyses.

Polycrystalline and single-crystalline Tb$_{2+x}$Ti$_{2-x}$O$_{7+y}$ samples were prepared by a standard solid-state reaction [34] and by a floating zone method [35]. Specific heat was measured by a quasiadiabatic method down to 0.1 K, using a plate-shaped crystal with a size of $0.7 \times 0.9 \times 0.1$ mm^3 whose shortest dimension is along a [110] axis. Magnetization was measured by a capacitive Faraday magnetometer using the same sample. Neutron scattering experiments were performed on NIST-BT7 [46] using a crystal sample cut from a neighboring part of the above sample and on ILL-IN5 [47] using the powder sample with $x = 0.005$ [34].

We first determine the magnitude of J_{nn} from the magnetic susceptibility χ_{exp}. The T dependence of χ_{exp} measured along the [111] direction on the single crystal shows an anomaly at $T_c = 0.53$ K [Fig. 2(a)]. While χ_{exp} is dominated by the contribution from the CF ground-state
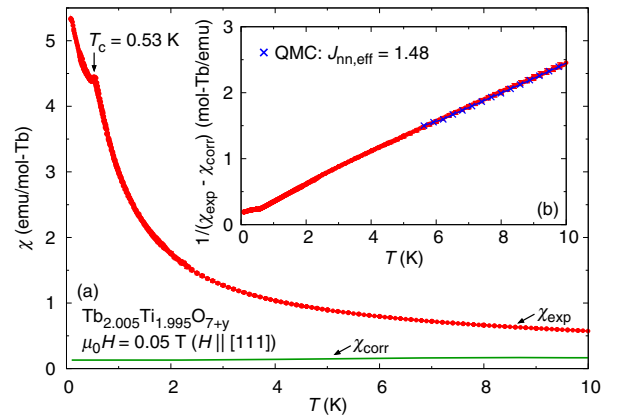

FIG. 2.　(a) Temperature dependence of magnetic susceptibility for an applied field along [111]. The solid line is χ_{corr} (see text for details). (b) Comparison between $[\chi_{exp} - \chi_{corr}]^{-1} = \chi_{gnd}^{-1}$ and QMC calculation. Note, 1 emu $= 10^{-3}$ A m^2.

doublets, a small but non-negligible correction χ_{corr} may arise from higher-energy CF states. Thus, we calculated χ_{corr} by taking the CF parameters of Ref. [36] and using a single-site approximation, i.e., using Eq. (2.1.18) of Ref. [48], where the contributions from the CF ground-state doublet are excluded. The χ_{corr} is also shown in Fig. 2(a). Now $\chi_{\mathrm{gnd}}\,(=\chi_{\mathrm{exp}}-\chi_{\mathrm{corr}})$ can be directly compared with a theoretical calculation based on the pseudospin-1/2 model Eq. (1). We have performed extensive QMC simulations [49,50] of the nearest-neighbor effective Hamiltonian $\mathcal{H}_{\mathrm{m,eff}}+\mathcal{H}_q$ on finite-size clusters up to 1024 pseudospins with typical Monte Carlo steps of 200 000. The experimental data (χ_{gnd}) are well reproduced by the QMC calculations in a wide range of δ and q, if we take $|J_{\mathrm{nn,eff}}| = 1.3$–$1.9$ K. Note that because of the negative sign problem of the QMC simulation, the analyses have been limited to a relatively high temperature range, $5 < T < 15$ K. In Fig. 2(b), we show a representative comparison between χ_{gnd} and the QMC results obtained for $(\delta, q) = (0, 0.85)$ as determined below. This comparison yields $J_{\mathrm{nn,eff}} = 1.48(1)$, leading to $J_{\mathrm{nn}} = 1.0(1)$ K. This value of $J_{\mathrm{nn,eff}}$ is of the same order as the previous estimation [51].

Next, we confirm the positive sign of $J_{\mathrm{nn,eff}}$ and extract the parameter values of (δ, q) from the comparison of the inelastic neutron scattering data. The previous inelastic magnetic neutron-scattering spectra measured on the $x = 0.005$ powder sample at $T = 0.1$ K $(\ll T_c)$, have shown a nearly flat broad peak at 0.1 meV in the (Q, E) space [34], as shown in Fig. 3(a). The peak is broader than the instrumental resolution, which suggests dispersive excitations. This experimental behavior can be described in terms of pseudospin waves in the PAF and PF phases, as discussed in Ref. [37]. The powder-averaged dynamical

magnetic structure factor $S(|\boldsymbol{Q}|, E)$ is calculated within the MF RPA [37], which can correctly describe the spectrum in an ordered state within the linear spin-wave approximation. Extensive calculations in a wide range of the parameters (δ, q) show that reasonable agreements are obtained in the PAF phase with $(\delta, q) = (0.0 \pm 0.4, 0.8 \pm 0.3)$ [Fig. 3(b)] and in the PF phase with $(\delta, q) = (-0.54 \pm 0.02, q < 1.1)$, when we fix $J_{\mathrm{nn}} = 1.0(1)$ K [Fig. 1(a)]. We note that only the cases of $J_{\mathrm{nn,eff}} > 0$ can reasonably reproduce the observed features for the case of the PAF phase [Fig. 3(b)]. The case of $J_{\mathrm{nn,eff}} < 0$ gives highly dispersive spectra that are not compatible with the experimental results [Fig. 3(c)].

Finally, we show, using CMC simulations of Eq. (1), that the parameter set showing the PAF explain reasonably well the observed specific heat $C_P(T, H)$ under weak [111] field while the other parameter set showing the PF does not. Figure 4(a) shows the T dependence of $C_P(T, H)$ under [111] field up to 1.0 T. The sharp peak at T_c survives only up to $\mu_0 H = 0.1$ T, turning into broad double peaks at 0.3 T. A full map of $C_P(T, H)$ is shown in Fig. 4(b). For comparison, maps of the calculated specific heat $C(T, H)$ by CMC simulations are presented in Figs. 4(c) and 4(d) for the same parameter choices as determined above, namely, $(\delta, q) = (0, 0.85)$ and $(-0.54, 0.5)$, respectively. Clearly, the PAF case shows a better qualitative agreement with the experiment, although with some discrepancy in the magnetic field and temperature scales. We note that CMC simulations with these PAF parameters also reproduce the experimental results of $C(T, H)$ under the [100] field [52].

One may not clearly see the change of states under the [111] field below 0.4 K in $C_P(T, H)$ [Figs. 4(a) and 4(b)]. However, certain changes are observed in the magnetization M. Figure 5(a) shows M-H curves at several temperatures under the [111] field. Two clear steplike kinks are observed at $\mu_0 H_1 \simeq 0.14$ and $\mu_0 H_2 \simeq 1.3$ T below the
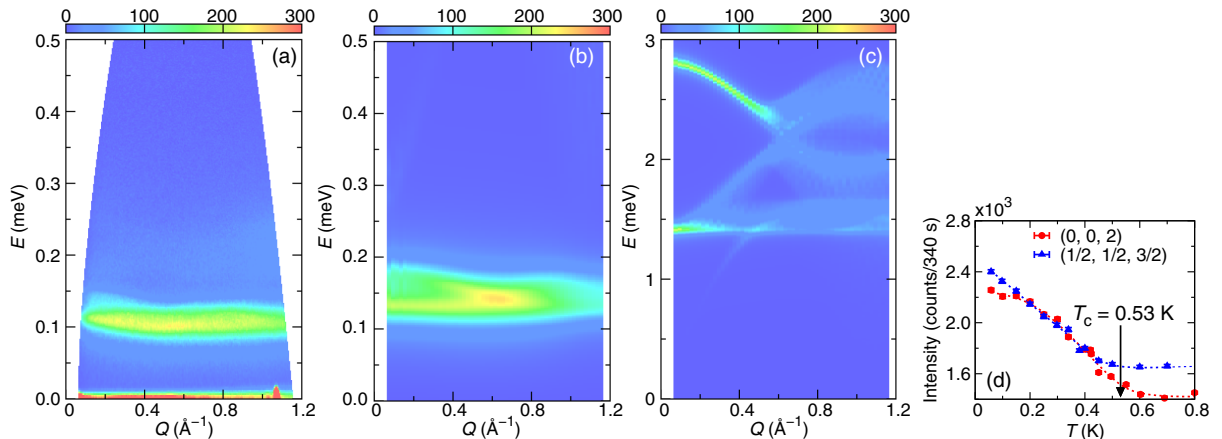

FIG. 3.   (a) Neutron inelastic magnetic spectra of the polycrystalline $\mathrm{Tb}_{2.005}\mathrm{Ti}_{1.995}\mathrm{O}_{7+y}$ sample taken at $T = 0.1$ K. (b) Calculated $S(Q, E)$ for the PAF phase with $J_{\mathrm{nn,eff}} > 0$ using $J_{\mathrm{nn,eff}} = 1.48$ K ($J_{\mathrm{nn}} = 1.00$ K) and $(\delta, q) = (0, 0.85)$. $J_{\mathrm{nn,eff}}$ is determined by the analysis of χ_{gnd}. (c) Calculated $S(Q, E)$ for the PAF phase with $J_{\mathrm{nn,eff}} < 0$ using $J_{\mathrm{nn,eff}} = -1.77$ K ($J_{\mathrm{nn}} = -2.25$ K) and $(\delta, q) = (-0.5, -1.0)$. $J_{\mathrm{nn,eff}}$ is determined by the analysis of χ_{gnd}. (d) T dependence of intensities of the single-crystal neutron Bragg scattering at (002) and $(\frac{1}{2}\frac{1}{2}\frac{3}{2})$.
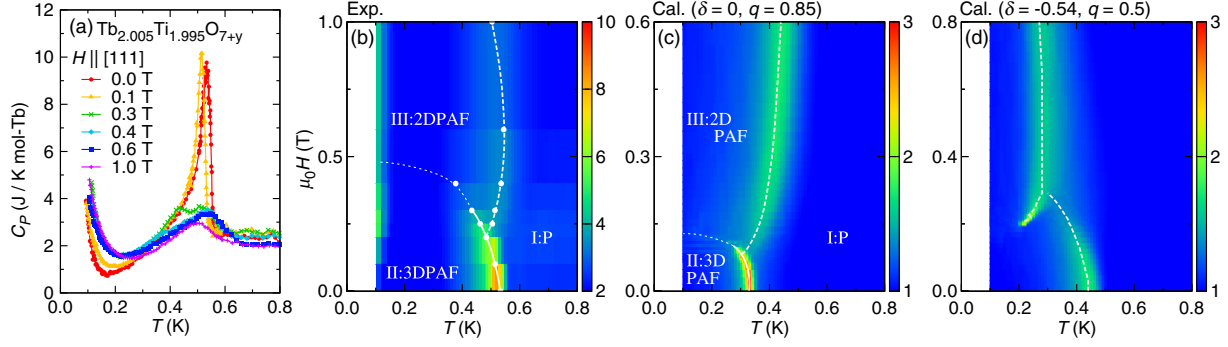
FIG. 4.   (a) Temperature dependence of the observed specific heat $C_P(T, H)$ for $H\|[111]$. (b) Temperature-field map of $C_P(T, H)$ for $H\|[111]$. Filled circles in the map are peak positions of $C_P(T, H)$. (c),(d) CMC results of specific heat $C(T, H)$ for (c) $(\delta, q) = (0, 0.85)$ with $J_{nn} = 1.00$ K and for (d) $(\delta, q) = (-0.54, 0.5)$ with $J_{nn} = 0.92$ K. The values of J_{nn} have been determined from the comparison of χ_{gnd} with the QMC results for each case. Solid, dashed, and dotted lines in (b), (c), and (d) are guides to the eyes. Labels in maps (b) and (c) indicate assigned states from the analysis with Eq. (1) and CMC simulations [40]; i.e., (I) a paramagnetic paraquadrupole state, (II) the 3D PAF state, and (III) the 2D PAF state.

zero-field T_c. CMC simulations with the same parameters as used above demonstrate the first kink at $\mu_0 H_1$ [Fig. 5(b)], indicating that it is a crossover or a phase transition from the three-dimensional (3D) PAF state [9] to the two dimensional (2D) PAF state [11,40]. This means that in intermediate fields ($\mu_0 H \simeq 0.5$ T), the system behaves as decoupled 2D kagomé layers of quadrupole moments separated by triangular layers of polarized magnetic moments. This bears resemblance to the kagomé ice state of SI materials [53]. In contrast, the second kink appears at a higher field than that of experiments at $\mu_0 H_2$. This result suggests that higher order terms neglected in Eq. (1), such as terms due to CF excited states [41], are required for further explanation of the behavior at fields higher than about 1 T.

All the above comparisons between the experiments and theories show that the LRO of TTO is the quadrupole order characterizing the PAF phase. Although this LRO cannot be detected directly through neutron Bragg scattering, we observed some indication of it. In fact, weak magnetic reflections are observed at the forbidden (002) position and at the superlattice $(\frac{1}{2}\frac{1}{2}\frac{3}{2})$ position [Fig. 3(d)]. Polarized neutron scattering experiments at BT7 confirm that both of them are magnetic. The long-range ordered magnetic moments of these reflections are roughly ~ 0.1 μ_B, which is too small to be the primary order parameter. We speculate that the (002) reflection appears simultaneously with the PAF order, whose order parameter is characterized by the wave vector $\boldsymbol{k} = 0$ [9,40], and is induced by higher order terms neglected in Eq. (1). On the other hand the $(\frac{1}{2}\frac{1}{2}\frac{3}{2})$ reflection, observed also in a powder sample [34], suggests a different origin because its T dependence is different from that of the (002) reflection [Fig. 3(d)].

Electric quadrupolar orders are related to the deformation of f-electron charge density. These naturally couple to displacements of ligand ions [48] and may induce cooperative JT effects and JT structural distortions [33,54].

Since the quadrupole-coupling terms of Eq. (1) are derived as the electronic coupling but are symmetry allowed terms under the space group of the pyrochlore lattice [11], these may contain a phonon-coupling contribution [55]. Thus, a direct detection of the quadrupole order (using resonant x-ray scattering) and/or of a small associated JT lattice distortion are difficult yet interesting topics for future investigations.

In summary, the hidden order of $Tb_{2+x}Ti_{2-x}O_{7+y}$ with $x = 0.005 > x_c$ has been studied using thermodynamic and neutron scattering measurements on single-crystalline and polycrystalline samples under the control of the off-stoichiometry of x. We take account of magnetic-dipole and electric-quadrupole moments of the CF ground-state doublet of the non-Kramers Tb^{3+} ion as well as the theoretically proposed quadrupole interaction [11]. Semiquantitative analyses of the experimental data based on a simple pseudospin-1/2 Hamiltonian demonstrate that the hidden order is an
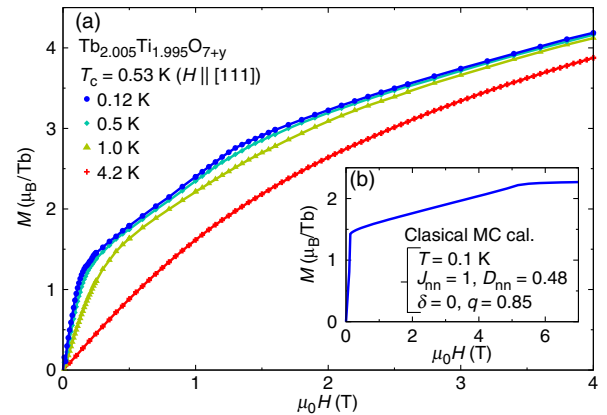

FIG. 5.   Field dependence of the magnetization M under the [111] magnetic field. (a) Experimental data on $Tb_{2.005}Ti_{1.995}O_{7+y}$ above and below $T_c = 0.53$ K. (b) CMC results obtained with the same parameters as for Figs. 3(b) and 4(c).

order of the electric quadrupole moments [Fig. 1(b)]. The estimated model parameters are located close to the phase boundary between the quadrupolar and U(1) QSL states. This result implies that the putative SL state of TTO studied for more than a decade is the U(1) QSL. Investigations in the context of a Higgs transition [9,10,56] and on the relation of it with the neighboring U(1) QSL phase using $Tb_{2+x}Ti_{2-x}O_{7+y}$ single crystals [35] are fascinating future topics.

[1] C. Lacroix, P. Mendels, and F. Mila, *Introduction to Frustrated Magnetism* (Springer, Berlin, Heidelberg, 2011).

[2] M. J. Harris, S. T. Bramwell, D. F. McMorrow, T. Zeiske, and K. W. Godfrey, Phys. Rev. Lett. **79**, 2554 (1997).

[3] S. T. Bramwell and M. J. P. Gingras, Science **294**, 1495 (2001).

[4] J. S. Gardner, M. J. P. Gingras, and J. E. Greedan, Rev. Mod. Phys. **82**, 53 (2010).

[5] A. P. Ramirez, A. Hayashi, R. J. Cava, R. Siddharthan, and B. S. Shastry, Nature (London) **399**, 333 (1999).

[6] I. A. Ryzhkin, JETP **101**, 481 (2005).

[7] C. Castelnovo, R. Moessner, and S. L. Sondhi, Nature (London) **451**, 42 (2008).

[8] M. Hermele, M. P. A. Fisher, and L. Balents, Phys. Rev. B **69**, 064404 (2004).

[9] S. B. Lee, S. Onoda, and L. Balents, Phys. Rev. B **86**, 104412 (2012).

[10] L. Savary and L. Balents, Phys. Rev. Lett. **108**, 037202 (2012).

[11] S. Onoda and Y. Tanaka, Phys. Rev. B **83**, 094411 (2011).

[12] Y.-P. Huang, G. Chen, and M. Hermele, Phys. Rev. Lett. **112**, 167203 (2014).

[13] M. J. P. Gingras and P. A. McClarty, Rep. Prog. Phys. **77**, 056501 (2014).

[14] H. R. Molavian, M. J. P. Gingras, and B. Canals, Phys. Rev. Lett. **98**, 157204 (2007).

[15] O. Benton, O. Sikora, and N. Shannon, Phys. Rev. B **86**, 075154 (2012).

[16] Y. Nambu, Phys. Rev. **117**, 648 (1960).

[17] P. W. Higgs, Phys. Rev. Lett. **13**, 508 (1964).

[18] P. W. Anderson, Phys. Rev. **130**, 439 (1963).

[19] E. Fradkin and S. H. Shenker, Phys. Rev. D **19**, 3682 (1979).

[20] D. S. Rokhsar and S. A. Kivelson, Phys. Rev. Lett. **61**, 2376 (1988).

[21] P. W. Anderson, Mater. Res. Bull. **8**, 153 (1973).

[22] P. A. Lee, Science **321**, 1306 (2008).

[23] L. Balents, Nature (London) **464**, 199 (2010).

[24] Y. Shimizu, K. Miyagawa, K. Kanoda, M. Maesato, and G. Saito, Phys. Rev. Lett. **91**, 107001 (2003).

[25] T.-H. Han, J. S. Helton, S. Chu, D. G. Nocera, J. A. Rodriguez-Rivera, C. Broholm, and Y. S. Lee, Nature (London) **492**, 406 (2012).

[26] J. S. Gardner, S. R. Dunsiger, B. D. Gaulin, M. J. P. Gingras, J. E. Greedan, R. F. Kiefl, M. D. Lumsden, W. A. MacFarlane, N. P. Raju, J. E. Sonier, I. Swainson, and Z. Tun, Phys. Rev. Lett. **82**, 1012 (1999).

[27] J. S. Gardner, A. Keren, G. Ehlers, C. Stock, E. Segal, J. M. Roper, B. Fak, M. B. Stone, P. R. Hammar, D. H. Reich, and B. D. Gaulin, Phys. Rev. B **68**, 180401 (2003).

[28] S. Petit, S. Guitteny, J. Robert, P. Bonville, C. Decorse, J. Ollivier, H. Mutka, and I. Mirebeau, EPJ Web Conf. **83**, 03012 (2015).

[29] M. Hirschberger, J. W. Krizan, R. J. Cava, and N. P. Ong, Science **348**, 106 (2015).

[30] A. J. Princep, H. C. Walker, D. T. Adroja, D. Prabhakaran, and A. T. Boothroyd, Phys. Rev. B **91**, 224430 (2015).

[31] S. Guitteny, I. Mirebeau, P. Dalmas de Réotier, C. V. Colin, P. Bonville, F. Porcher, B. Grenier, C. Decorse, and S. Petit, Phys. Rev. B **92**, 144412 (2015).

[32] Y.-J. Kao, M. Enjalran, A. Del Maestro, H. R. Molavian, and M. J. P. Gingras, Phys. Rev. B **68**, 172407 (2003).

[33] P. Bonville, I. Mirebeau, A. Gukasov, S. Petit, and J. Robert, Phys. Rev. B **84**, 184409 (2011).

[34] T. Taniguchi, H. Kadowaki, H. Takatsu, B. Fak, J. Ollivier, T. Yamazaki, T. J. Sato, H. Yoshizawa, Y. Shimura, T. Sakakibara, T. Hong, K. Goto, L. R. Yaraskavitch, and J. B. Kycia, Phys. Rev. B **87**, 060408(R) (2013).

[35] M. Wakita, T. Taniguchi, H. Edamoto, H. Takatsu, and H. Kadowaki, J. Phys. Conf. Ser. **683**, 012023 (2016).

[36] I. Mirebeau, P. Bonville, and M. Hennion, Phys. Rev. B **76**, 184436 (2007).

[37] H. Kadowaki, H. Takatsu, T. Taniguchi, B. Fåk, and J. Ollivier, SPIN **05**, 1540003 (2015).

[38] B. C. den Hertog and M. J. P. Gingras, Phys. Rev. Lett. **84**, 3430 (2000).

[39] S. V. Isakov, R. Moessner, and S. L. Sondhi, Phys. Rev. Lett. **95**, 217201 (2005).

[40] H. Kadowaki *et al.* CMC simulations, based on the single-spin-flip Metropolis algorithm, will be published in a separate paper.

[41] See Supplemental Material at http://link.aps.org/supplemental/10.1103/PhysRevLett.116.217201 for the effect of higher excited CF states in the analysis of the magnetization and for the result of inelastic neutron scattering data above T_c, which includes Refs. [42–44].

[42] Y. Tabata, H. Kadowaki, K. Matsuhira, Z. Hiroi, N. Aso, E. Ressouche, and B. Fak, Phys. Rev. Lett. **97**, 257205 (2006).

[43] A. Bertin, Y. Chapuis, P. D. de Reotier, and A. Yaouanc, J. Phys. Condens. Matter **24**, 256003 (2012).

[44] J. Zhang, K. Fritsch, Z. Hao, B. V. Bagheri, M. J. P. Gingras, G. E. Granroth, P. Jiramongkolchai, R. J. Cava, and B. D. Gaulin, Phys. Rev. B **89**, 134410 (2014).

[45] H. Kusunose, J. Phys. Soc. Jpn. **77**, 064710 (2008).

[46] J. W. Lynn, Y. Chen, S. Chang, Y. Zhao, S. Chi, W. Ratcliff II, B. G. Ueland, and R. W. Erwin, J. Res. Natl. Inst. Stand. Technol. **117**, 61 (2012).

[47] J. Ollivier and H. Mutka, J. Phys. Soc. Jpn. **80**, SB003 (2011).

[48] J. Jensen and A. R. Mackintosh, *Rare Earth Magnetism* (Clarendon Press, Oxford, 1991).

[49] Y. Kato and S. Onoda, Phys. Rev. Lett. **115**, 077202 (2015).

[50] Y. Kato and N. Kawashima, Phys. Rev. E **79**, 021104 (2009).

[51] M. J. P. Gingras, B. C. den Hertog, M. Faucher, J. S. Gardner, S. R. Dunsiger, L. J. Chang, B. D. Gaulin, N. P. Raju, and J. E. Greedan, Phys. Rev. B **62**, 6496 (2000).

[52] H. Takatsu, T. Taniguchi, S. Kittaka, T. Sakakibara, and H. Kadowaki, J. Phys. Conf. Ser. **683**, 012022 (2016).

[53] K. Matsuhira, Z. Hiroi, T. Tayama, S. Takagi, and T. Sakakibara, J. Phys. Condens. Matter **14**, L559 (2002).

[54] G. A. Gehring and K. A. Gehring, Rep. Prog. Phys. **38**, 1 (1975).

[55] A. P. Sazonov, A. Gukasov, H. B. Cao, P. Bonville, E. Ressouche, C. Decorse, and I. Mirebeau, Phys. Rev. B **88**, 184428 (2013).

[56] L. J. Chang, S. Onoda, Y. Su, Y.-J. Kao, K.-D. Tsuei, Y. Yasui, K. Kakurai, and M. R. Lees, Nat. Commun. **3**, 992 (2012).